High-Power Density Experiments in a Shock-Tunnel MHD Generator

A. Veefkind, *J. W. M. A. Houben,* J. H. Blom,* and L. H. T. Rietjens*
Eindhoven University of Technology, Eindhoven, Netherlands

An experimental MHD generator facility is described, in which cesium-seeded argon is used as a working medium. The heating of the gas is realized by compression in a shock tunnel. The enthalpy input into the generator is 5 MW. The test time is 5 msec. The objective of the experiments has been the achievement of electrical energy extractions as high as expected from one-dimensional channel computations. The effects of voltage drops and short-circuiting of the Hall field on the power output are discussed, and the performances of a 3ℓ and a 10ℓ channel are examined. In both cases, agreement between the experiment and the theoretical model was found. The 10ℓ channel yielded an enthalpy extraction of 24% with an electrical power density of 140 MW/m^3.

I. Introduction

A CONSIDERABLE variety of experiments in MHD generators with seeded noble gases as media have been carried out during the last 10 years.[1,2] These experiments have shown that enhanced electron temperatures and significant nonequilibrium ionization can be achieved. They also show that a number of loss mechanisms, such as voltage drops, segmentation losses, reduction of the Hall field, and instabilities, limit the electrical power output.

Experimental generators employing shock tubes as plasma production systems are suitable for experiments directed to closed-cycle MHD energy conversion, particularly when a high thermal input power has to be considered. Then, larger channels can be used, in which the bulk phenomena are not dominated by the wall effects.[3-5] Therefore, the processes in these channels are, in first order, appropriate to be described by a quasi-one-dimensional model.

The experiments discussed here concern an experimental MHD generator with a total input power of about 5 MW. They are directed toward high enthalpy extraction and high power densities. The experimental results will be compared with a one-dimensional channel analysis. Particular attention will be given to the losses. Since the channels employed are still small compared to the eventual commercial MHD ducts, voltage drops are a very important loss mechanism. In some specific experiments, the influence of material and geometrical effects on the voltage drops has been examined.

II. Experimental Arrangement

The production of plasmas for MHD generators in shock tunnels is a technique that is used in several places. Compare, for instance, Ref. 6 with the experiment described here. The shock tunnel employed[7,8] has a cross-section diameter of 22.4 cm (Fig. 1). It consists of a driver section of 4 m and a test section of 8 m, separated from each other by a double diaphragm. The driven end of the shock tube is closed off by an endplate in which a 7-$\times$9-cm^2 hole connects the test section with the nozzle of the MHD generator. The argon-cesium mixture is compressed to reach a stagnation pressure of 7.5 bar and a stagnation temperature of about 3400°K. The shock tunnel is operated in the tailored interface mode to obtain the maximum test time of 5 msec.

This paper refers to two different channel geometries, quoted as the 3ℓ channel and the 10ℓ channel. The 3ℓ channel is combined with a Mach 1.8 nozzle, and the 10ℓ channel with a Mach 1.6 nozzle. The 3ℓ channel consists of two parts. The upstream part, with a length of 10 cm, has a constant duct area of 7 $\times$ 9 cm^2. It contains six pairs of cylindrical electrodes, which can be heated electrically. The downstream part is diverging from 7 $\times$ 9 to 9 $\times$ 9 cm^2 over a length of 40 cm, where the electrode walls are diverging. The stainless-steel electrodes here cannot be heated. Throughout the channel the electrode cylinders have a length of 8.5 cm and a diameter of 4 mm. The pitch is 1.4 cm, and the centerline of each electrode is at a distance of 4 mm from the adjacent wall.

The 10ℓ channel diverges from 5 $\times$ 14 to 14 $\times$ 14 cm^2 over a length of 80 cm, but there the insulator walls are diverging and the electrode walls parallel. This arrangement has been chosen because it results in a relatively constant current per electrode pair along the channel for equally loaded electrodes. Another advantage is the more constant load factor along the channel, despite a decreasing conductivity toward the exit. The electrodes are cylindrical, made of stainless-steel, with a diameter of 4 mm and lengths varying from 5 to 14 cm. The centerline of each electrode is at a distance of 4 mm from the adjacent wall.

Two different magnets are used, one in conjunction with the 3ℓ channel and one in conjunction with the 10ℓ channel. For both magnets, the maximum magnetic induction attained was about 3.5 T. The 10ℓ channel magnet has no significant variation of magnetic induction throughout the 80-cm length of the generator, whereas the 3ℓ channel magnet shows a slight inhomogeneity at the ends of the duct.

The stagnation pressure in the shock tunnel behind the reflected shock is measured with a piezoelectric pressure transducer. Sets of voltage probes, located flush with the insulator walls, provide information about the voltage distribution in the channel. A modified line-reversal measurement[9] is used to determine the electron temperature and the seed atom density. Continuum radiation, originating from two particles recombinations, is measured at 4893 and 4102 Å to determine the electron temperature and the electron density.

III. Analysis

The gasdynamical entrance conditions are calculated from the stagnation temperature and the stagnation pressure assuming isentropic expansion in the nozzle. The electron temperature and density are determined from the electron energy balance, Saha's equation, and Ohm's law, as described

Received Dec., 23, 1975; revision received April 1, 1976.

The authors wish to express their thanks to G. Huijgen, H. F. Koolmees, J. W. Peters, and J. P. Verhagen for their assistance in the construction and operation of the facility and for their contribution in the data acquisition and optical diagnostics.

Index categories: Plasma Dynamics and MHD; Electric Power Generation Research.

*Staff Members, Group Direct Energy Conversion, Department of Electrical Engineering.

in Ref. 3. For all runs, a seed fraction of 4.5×10^{-4} was consistent with these calculations and also with the results of the recombination radiation measurements.

A quasi-one-dimensional analysis is used to describe the behavior of the flow. Again the electron gas is assumed to obey the electron energy balance equation and Saha's equation. Finite segmentation, instabilities, radiation losses, friction, and cooling by the generator walls have been taken into account according to Ref. 7. The voltage drop has been assumed to increase linearly with the generator distance, fitting the experimental values obtained at two positions.

IV. Experimental Results

General

The objective of the experiments discussed here has been to obtain specific powers and enthalpy extractions as high as expected from the theory. For the 3ℓ channel, the one-dimensional theory described before yields a specific power level ranging from 50 to 100 MW/m^3, depending on the voltage drop. In case of the 10ℓ channel, a specific power between 100 and 150 MW/m^3 theoretically is expected. The theoretical enthalpy extractions for the magnetic inductions attainable are 6% for the 3ℓ channel and 20% for the 10ℓ channel.

It has been tried to understand the influence of electrode geometry and electrode material on the generator performance from a number of specific experiments in which the electrode material, the electrode diameter, the electrode mutual distance, and the electrode distance from the wall have been varied. To investigate the influence of electrode temperature, the voltage drops are observed as a function of electrode temperature. Typical channel entrance conditions are $p=1.3$ bar, $u=1400$ m/sec, and $T=1725°K$ in the 3ℓ channel, and $p=1.5$ bar, $u=1260$ m/sec, and $T=1800°K$ in the 10ℓ channel.

Voltage Drops

Specific experiments have been carried out to examine the dependence of the voltage drop on the electrode material, the diameter of the rods, hydrodynamic effects, and the electrode surface temperature. A channel, especially made for this purpose, contained tungsten and stainless-steel electrodes, both of 2- and 4-mm diam. Two electrode pairs (one of 2- and one of 4-mm diam) have been located protruding into the core flow. The voltage drops were evaluated from the voltage distributions between cathodes and anodes as measured with voltage probes. Experiments in the channel mentioned have shown the following:

1) The value of the total voltage drop at the anode and the cathode is not dependent on whether tungsten or stainless steel is used as electrode material.

2) The value of the voltage drop is not sensitive to the diameter of the rod-type electrodes. This can be concluded by observing that, for electrodes with Ø 2 and Ø 4 mm for similar plasma velocity and magnetic induction, equal Faraday currents and equal bulk and boundary-layer resistances are found.

3) At electrode pairs protruding into the core flow, the voltage drop is lower. From the observed open voltages, it can be concluded that the bulk velocity is reduced at the electrodes that stick into the core out of the boundary layers of the upstream electrodes. At this location, the internal as well as the boundary-layer resistances are reduced significantly. It could not be determined whether the effect mentioned is due to a change in the hydrodynamic conditions or to a change in the current distribution pattern.

The effect of the electrode temperature was studied in the upstream section of the 3ℓ channel. In consecutive runs, electrode temperatures of 300°, 1200°, 1250°, 1300°, 1350°, and again 300°K have been applied. No decrease of voltage drops

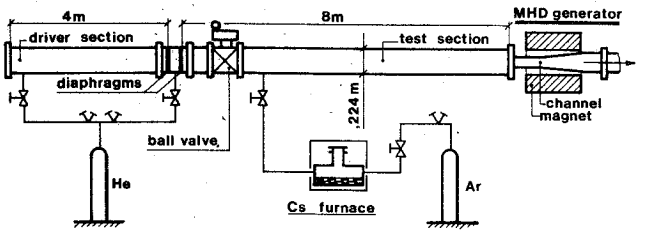

Fig. 1 Layout of the shock-tunnel experiment.

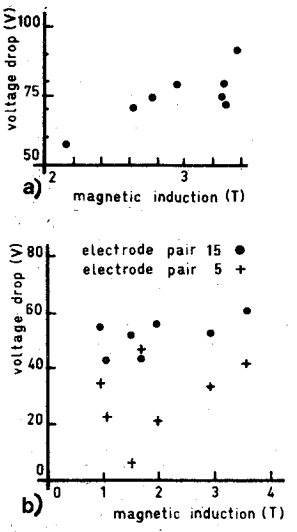

Fig. 2 Voltage drop vs magnetic induction a) in the 3ℓ channel at the ninth electrode pair of the downstream section, and b) in the 10ℓ channel at the fifth and fifteenth electrode pair.

resulted from increasing electrode surface temperatures. The Langmuir S-curves in Ref. 10 show that the current levels involved in our experiments are too high to expect homogeneous emission, although they have been kept as low as 1 A/cm^2 deliberately. Thus, an increase of currents at higher electrode temperatures cannot be expected from the Langmuir S-curves.

Voltage drops, measured in the 3ℓ channel during the runs carried out to study its power production, are given as a function of the magnetic induction in Fig. 2a. The voltage drop is measured at the ninth electrode pair of the downstream section. Although there is some tendency for the voltage drop to increase with the magnetic induction, the effect is weak, and with only two exceptions the voltage drop values stay between 70 and 80 V. For the runs carried out in the 10ℓ channel to study the electrical power production, the voltage drops measured at the electrode pairs 5 and 15 are presented in Fig. 2b for various values of the magnetic induction. Here also, there is no significant increase of the voltage drop with the magnetic induction.

In conclusion, it can be stated that arcing is the most likely discharge mechanism of the discharge at the electrode surface. This explains the insensitivity of the voltage drop to the electrode material, the diameter of the rods, and the electrode temperature. How the measured voltage drops are affected by the hydrodynamic conditions and by the current distribution close to the electrodes has not become clear from the experiments, although they show that at least one of the two effects is important.

Current Distribution Along the Channel

Current distributions along the 3ℓ channel are shown in Fig. 3, together with Hall voltage distributions. The graphs show agreement between the calculated curves and the experimental points. The calculated current levels, however, depend strongly on input data as the values of the voltage drop, the Hall voltage, the critical Hall parameter, and the reduction

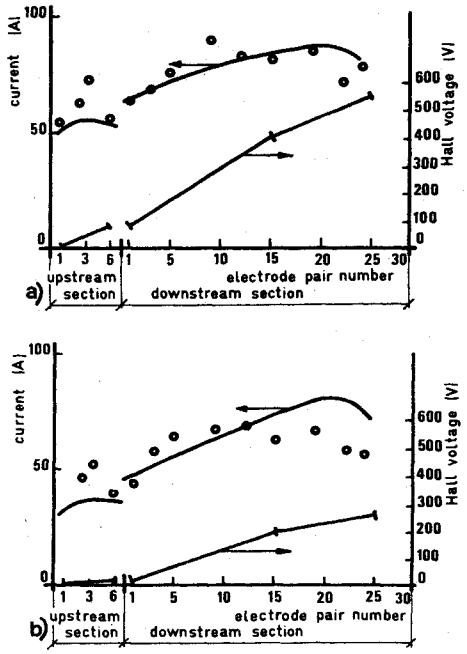

Fig. 3 Current and Hall voltage along the 3ℓ channel: a) run 1203, $B=2.94$ T, Hall current = 83 A; and b) run 1193, $B=3.29$ T, Hall current = 207 A.

factor because of finite segmentation. The trend of the current distribution in the case of the lower magnetic induction is somewhat better than at the higher magnetic induction. The discrepancy in the case of the higher B field coincides with a reduction in Hall field due to shorting.

For the 10ℓ channel, the current along the generator is plotted in Fig. 4. Here also, the calculated current level is very sensitive for the input data mentioned. Run 1232 with a magnetic induction of only 1.07 T shows an increase of current in the first part of the duct, which is not explained by the calculations. This apparent relaxation effect cannot be understood from one-dimensional electron density relaxation theory, which yields much smaller relaxation lengths. Two-dimensional calculations cannot account for the observed change in relaxation lengths with the magnetic induction, since the two-dimensional description predicts a relaxation length independent of B.[7] A variation in current caused by a dependence of the voltage drop on the current density seems more likely at these relatively small values of the induced field. The agreement between theory and experiment as shown in the other graphs of Fig. 4 is typical for all runs with a magnetic induction above 1 T.

It can be seen from Figs. 3 and 4 that, apart from the runs at low magnetic inductions, no significant ionization relaxation region appears at the channel entrance, neither in the 3ℓ nor in the 10ℓ channel. No preionization has been applied to these experiments, but it should be noted that the high stagnation temperatures employed have a positive influence on the entrance conductivity.

Hall Fields

In all runs discussed, the microscopic Hall parameter is larger than the critical value related to ionization instabilities. Hence, the Hall field is reduced, and its dependence on the magnetic induction is no stronger than linear. This effect has been taken into account in the calculations by the introduction of a constant effective Hall parameter. A further reduction of the Hall field is caused by Hall currents. Since the instabilities change the effective value of the conductivity as well, which the axial currents do not, it is possible to make some distinction between the two effects by comparing the experimental results with the calculations. As a result, a value of 1.5 has been adopted for the effective Hall parameter, and any further reduction of the Hall field has been attributed to the existence of Hall currents.

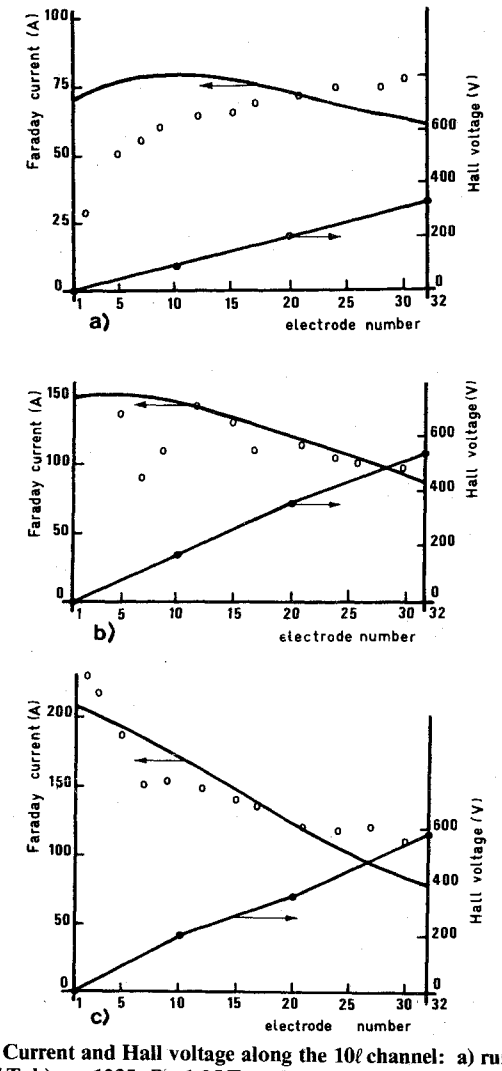

Fig. 4 Current and Hall voltage along the 10ℓ channel: a) run 1232, $B=1.07$ T; b) run 1235, $B=1.95$ T; and c) run 1240, $B=2.93$ T.

The location of the electrodes free from the wall is, in general, favorable to reach high Hall fields, and so is the cylindrical geometry. If the flow velocity in between the electrodes is low, it can be expected from two-dimensional calculations[8] that the electrode spacing of 1 cm in case of the 3ℓ channel, as well as the 2.1 cm in case of the 10ℓ channel, is large enough to prevent shorting through highly conductive plasma layers.

In the 3ℓ channel, Hall fields up to 1040 V/m were measured. The highest fields were measured at a magnetic induction slightly below 3 T. Above 3 T, Hall shorting occurred, which also could be seen from the Hall voltage history as recorded on scope. In cases of low Hall current, as in run 1203, the Hall field was about constant along the channel, as shown in Fig. 3a. In cases of significant reduction of the Hall field due to shorting, as run 1193, the Hall field in the upstream section was smaller than in the downstream section (Fig. 3b), suggesting an internal Hall current loop in the upstream section.

In the 10ℓ channel, external shorting has been prevented by careful insulation from ground of the downstream end of the generator and the expansion tank. To check this insulation during a run, the voltage at the expansion tank was monitored. The measured voltage then equals the Hall voltage across the generator during the test time and does not show any indication of shorting during the run. The Hall voltage shows a linear increase along the generator duct (Fig. 4), and

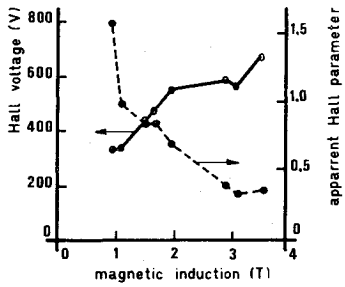

Fig. 5 Total Hall voltage and apparent Hall parameter vs magnetic induction in the 10ℓ channel

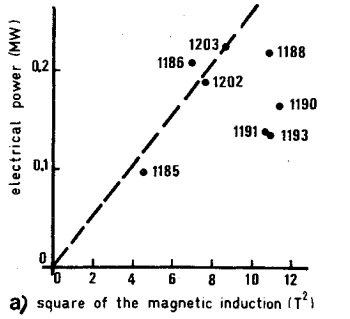

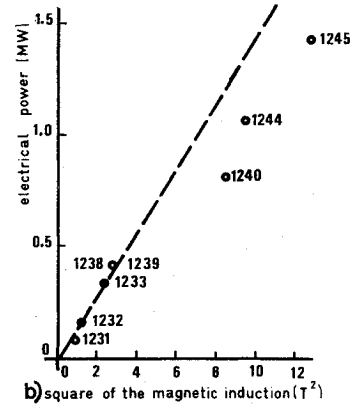

Fig. 6 Electrical power vs the square of the magnetic induction: a) 3ℓ channel; and b) 10ℓ channel.

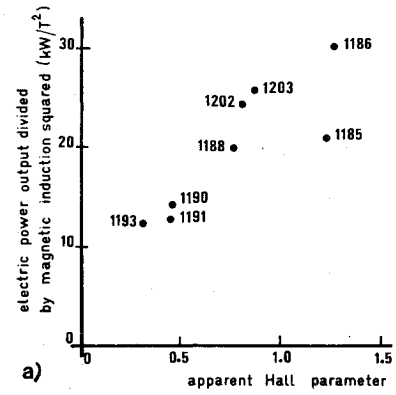

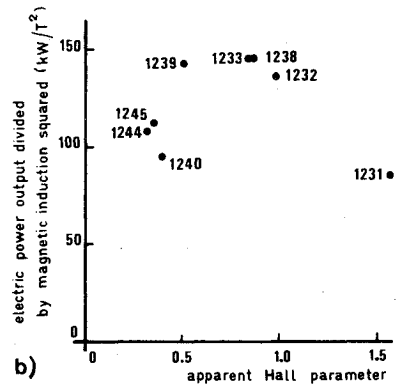

Fig. 7 Electrical power divided by the square of the magnetic induction vs the apparent Hall parameter: a) 3ℓ channel; and b) 10ℓ channel.

this is typical for all runs, indicating either the absence of internal shorting or a shorting that is distributed equally along the generator. Figure 5 shows that the Hall voltage in the 10ℓ channel keeps increasing with the magnetic induction, which was not the case in the 3ℓ channel. The Hall field, however, is lower than in the 3ℓ channel. No field larger than 900 V/m has been measured. The apparent Hall parameter is determined by voltage probe measurements of E_x and E_y. Figure 5 shows a considerable decrease of the apparent Hall parameter with increasing magnetic induction. This means that either axial shorting is present or that the direction of the current path changes with the B field, resulting in a larger J_x component at

Table 1 Generator performance

Channel	Run	Magnetic induction, T	Thermal input, MW	Mass flow, kg/sec	Electrical output, MW	Enthalpy extraction, %	Electrical power density, MW/m³
a) 3ℓ							
	1185	2.14	4.1	2.2	0.096	2.3	36
	1186	2.62	4.2	2.3	0.208	5.0	77
	1188	3.29	4.3	2.3	0.216	5.0	80
	1190	3.38	4.2	2.3	0.164	3.9	61
	1191	3.27	3.2	2.0	0.138	4.3	51
	1193	3.29	4.1	2.3	0.135	3.3	50
	1202	2.76	4.3	2.3	0.187	4.3	69
	1203	2.94	4.2	2.3	0.223	5.3	83
b) 10ℓ							
	1231	0.95	5.8	3.4	0.077	1.3	7.7
	1232	1.07	6.1	3.5	0.16	2.5	16
	1233	1.50	5.8	3.4	0.33	5.7	33
	1238	1.68	5.7	3.4	0.41	7.1	41
	1239	1.68	5.9	3.4	0.41	6.9	41
	1240	2.93	5.9	3.4	0.81	14	81
	1244	3.12	5.9	3.4	1.1	18	110
	1245	3.57	5.9	3.4	1.4	24	140

the axis. As mentioned before, there is no clear indication of axial shorting. It was not possible to determine the direction of the current density at the axis accurately because of the limited number of potential probes in the channel.

Electrical Output and Enthalpy Extraction

Table 1 gives the electrical power output for the runs discussed here. Simple theory predicts a linear dependence between the electrical output and the square of the magnetic induction. Figures 6a and 6b show that this rule holds for low magnetic fields. At larger values of the magnetic induction, this relationship fails due to Hall currents. This is demonstrated in Figs. 7a and 7b, which show the electrical power divided by the square of the magnetic field in relation to the measured apparent Hall parameter. The low specific powers of runs 1185 and 1231 at high values of the specific Hall parameters presumably are to be attributed to the relatively high voltage drops at low magnetic inductions. Table 1 gives also the thermal input of the generator, the enthalpy extraction, and electrical power density. It is seen that an enthalpy extraction of 24% and a power density of 140 MW/m^3 are reached despite the low value of the apparent Hall parameter of 0.4

V. Conclusions

The measured current distribution is in fairly good agreement with the one-dimensional computations, if, apart from the entrance conditions, appropriate values for the voltage drops, the critical Hall parameter, the Hall current, and the current reduction due to finite segmentation are given. No complete model of the voltage drops could be constructed. It is demonstrated, however, that the discharge through the boundary layer is maintained by arcing in the cases of interest. Furthermore, the value of the voltage drop is determined by the conditions of the hydrodynamical boundary layer and by the current density distribution near the electrode considered.

High specific power levels (140 MW/m^3) and large enthalpy extractions (24%) have been reached in the 10ℓ channel. The electric power is reduced by Hall shorting for a magnetic induction $B>3$T. The observed increase in enthalpy extractions from 5 to 24%, by scaling the channel from 3 to 10ℓ, could be explained fully by the theoretical model used.

References

[1] "MHD Electrical Power Generation 1972 Status Report," *Atomic Energy Review*, Vol. 10, No. 3. 1972.

[2] Brederlow, G., Witte, J. J., and Zinko, H., "Performance of a Faraday Rare Gas Alkali MHD Generator," *AIAA Journal*, Vol. 12, April 1974, pp. 481–489.

[3] Blom, J. H., et al., "High Power Density Experiments in the Eindhoven Shock Tunnel MHD Generator," *Proceedings of the 6th International Conference on MHD*, Vol. 3, 1975, pp. 73–88.

[4] Shioda, S., et al., "Performance of a Faraday MHD Generator with a Supersonic Seeded Helium," *Proceedings of the 6th International Conference on MHD*, Vol. 3, 1975, pp. 63–72.

[5] Marston, C., et al., "Large Enthalpy Extraction Results in a Nonequilibrium MHD Generator," *Proceedings of the 6th International Conference on MHD*, Vol. 3, 1975, pp. 89–104.

[6] Zauderer, B. and Tate, E., "Electrode and Gasdynamic Effects in a Large Nonequilibrium MHD Generator," *AIAA Journal*, Vol. 11, Feb., 1973, pp. 149–155.

[7] Blom, J. H., "Relaxation Phenomena in an MHD Generator with Pre-ionizer," Thesis, 1973, Eindhoven University of Technology, Eindhoven, Netherlands.

[8] Houben, J. W. M. A., "Loss Mechanisms in an MHD Generator," Thesis, 1973, Eindhoven University of Technology, Eindhoven, Netherlands.

[9] Van Ooyen, M. H. F., and Houben, J. W. M. A., "Determination of the Electron Temperature of a Shocktunnel-Produced Ar-Cs Plasma by the Line Reversal Method Using Non-Resonance Lines of Cs," *Journal of Quantitative Spectroscopy and Radiative Transfer*, Vol. 14, June 1974, pp. 395–403.

[10] Taylor, J. B. and Langmuir, I., "The Evaporation of Atoms, Ions, and Electrons from Caesium Films on Tungsten," *Physical Review*, Vol. 44, Ser. 2, 1933, pp. 423–458.